

An analytical model of pneumatic suspensions based on an experimental characterization

A.J. Nieto*, A.L. Morales, A. González, J.M. Chicharro, P. Pintado

*Área de Ingeniería Mecánica, E.T.S.I. Industriales, Universidad de Castilla-La Mancha,
Avda Camilo José Cela s/n, 13071 Ciudad Real, Spain*

Received 28 March 2007; received in revised form 8 November 2007; accepted 12 November 2007
Available online 21 December 2007

Abstract

We present an analytical model of air spring suspensions that is based on an experimental characterization. The suspension consists of three principal parts: the air spring, an auxiliary tank, and a pipe connecting the two. An analytical nonlinear fluid dynamics model is first analyzed, modeling the suspension stiffness, damping factor, and transmissibility. The model is then linearized and this linear version is studied in depth, finding that the behavior of the suspension as reflected in the aforementioned three characteristics is strongly dependent on the size of the three suspension parts. The analysis allows us to propose a practical strategy for the operation of the suspension.

© 2007 Elsevier Ltd. All rights reserved.

1. Introduction

The development of machinery and vehicles has increased the need for mechanical elements that are able to eliminate undesired vibrations. All vehicle suspensions are designed with the same end, i.e., to filter out vibrations coming from the tyre in contact with the road. One such suspension, the air suspension, has certain advantages over the classical mechanical suspensions in minimizing road wear and increasing passenger comfort. It is well known that air suspensions can provide both a soft ride at low speed on good roads and stability and control on rough roads at high speed. Moreover, the vehicle's chassis height can be adjusted to suit the particular conditions of any given trip [1].

The usefulness of pneumatic systems was demonstrated in Ref. [2], which addressed the problem of vibrations caused by vehicle cabins and their effect on the human body. The study showed that the need to add isolation to the vehicle cabins in order to prevent harmful vibrations from reaching the passengers was better served by seats with air suspension which attenuates frequencies above 4 Hz better than traditional suspension systems. Other studies have found benefits in air suspensions for seats in agricultural machinery [3,4] and in pneumatic systems in vibratory hand tools [5].

The use of a resistance (discharge orifice) between an air spring and a chamber as a dissipation element to increase damping has been considered in several studies (an example is Ref. [6]). Although its practicality has

*Corresponding author.

E-mail address: antoniojavier.nieto@uclm.es (A.J. Nieto).

Nomenclature			
A_s	spring effective area (m ²)	P_r	relative pressure at the reservoir (bar)
C_r	the pipe restriction coefficient (N ⁵ /m/s)	P_s	relative pressure at the air spring (bar)
D_p	the pipe's cross-section diameter (m)	R	gas constant for air (J/kg/K)
F	force exerted at the air spring (N)	T	air suspension temperature (K)
g	acceleration due to gravity (m/s ²)	V_r	reservoir volume (m ³)
k	pneumatic suspension total stiffness (N/m)	V_s	air spring volume (m ³)
k_{as}	air spring effective area stiffness (N/m)	V_{sr}	reservoir plus spring volume (m ³)
k_s	air spring stiffness (N/m)	x	absolute response (m)
k_{vs}	air spring volume stiffness (N/m)	y	excitation (m)
k_{vsr}	pneumatic suspension volume stiffness (N/m)	z	suspension height (m)
l_p	the pipe length (m)	z_0	initial height for the air spring (m)
\dot{m}	mass flow rate (kg/s)	γ	specific heat ratio
M	sprung mass (kg)	ε	dimensionless parameter
n	polytropic coefficient	θ	dimensionless parameter
		μ	dynamic viscosity of air (Pa s)
		ρ	density of air (kg/m ³)
		ω_{tr}	transition frequency (rad/s)

been questioned [7] because the level of damping is amplitude dependent and unsuited to linear modeling [8], this damping element has been used to simulate with nonlinear techniques the behavior of an ambulance stretcher fitted with a rigid wall linear cylinder air suspension [9], and to separate two chambers in a vibration isolator [10]. Another commonly used method of flow resistance is to include a valve with two parallel plates which restrict the air flow through the air suspension [1]. Nevertheless, these devices may be too cumbersome when there is need to implement a control strategy that modifies the suspension's characteristics.

There are several ways to incorporate said air spring suspensions. For example, in works like Ref. [11], a rigid wall pneumatic linear actuator is presented in parallel with an helical spring. The present work describes an air spring suspension with different pipes selected as the dissipation element together with an auxiliary volume. We study the system theoretically with both nonlinear and linear models, and show how the linear model naturally suggests a specific control strategy.

2. Nonlinear model

The pneumatic suspension we considered consists of three principal parts. The first is an air spring, the second component is a rigid tank and the third is a pipe connecting the first two elements. Consider first a closed system that includes only the air spring. The force exerted by the air spring can be written

$$F = P_s A_s, \quad (1)$$

i.e., that the force is proportional to the air spring internal pressure, P_s , and the air spring effective area, A_s . The air spring stiffness can be defined as the derivative of this force with respect to the air spring height z (defined as the difference between the response x and the excitation y plus an initial height value z_0):

$$k_s = -\frac{dF}{dz} = -\left[A_s \frac{dP_s}{dz} + P_s \frac{dA_s}{dz} \right]. \quad (2)$$

A polytropic transformation, $P_s V_s^n = \text{const}$, is assumed between an initial state (denoted by the additional subscript 0) and a final state. The derivative of air spring pressure with respect to height is then

$$\frac{dP_s}{dz} = -\frac{n P_{s0} V_{s0}^n}{V_s^{n+1}} \frac{dV_s}{dz}, \quad (3)$$

where P_{s0} and V_{s0} are the air spring initial pressure and volume, respectively. The air spring stiffness can now be written as

$$k_s = \frac{nP_{s0}V_{s0}^n A_s}{V_s^{n+1}} \frac{dV_s}{dz} - P_s \frac{dA_s}{dz}. \quad (4)$$

By defining k_{as} and k_{vs} as

$$k_{as} = -P_s \frac{dA_s}{dz}, \quad (5)$$

$$k_{vs} = \frac{nP_{s0}V_{s0}^n A_s}{V_s^{n+1}} \frac{dV_s}{dz} \quad (6)$$

the air spring stiffness can be written as the sum of two terms: a stiffness term, k_{as} , due to the air spring effective area variation with height z , and a volume term, k_{vs} , which depends on the air spring volume variation with height z .

As was mentioned above, the stiffness k_s corresponds to a closed system consisting of the air spring alone, i.e., the auxiliary reservoir has not as yet been taken into account in the model. Nevertheless, the pressures in the air spring and the reservoir can be assumed to be the same at any given instant (provided that the pipe connecting the two chambers is open) if the suspension dynamics are sufficiently slow. If this assumption holds, one can use Eq. (4) to obtain the suspension stiffness, k , by adding the tank volume (V_r) to that of the spring:

$$k = \frac{nP_{s0}V_{sr0}^n A_s}{V_{sr}^{n+1}} \frac{dV_s}{dz} - P_s \frac{dA_s}{dz}, \quad (7)$$

where V_{sr} is the sum of the volume of the air spring, V_s , and the tank volume, V_r and, thus, V_{sr0} is the initial sum of volumes. In this case, the pneumatic suspension stiffness is $k = k_{as} + k_{vsr}$, and the stiffness term due to the suspension volume variation with respect to height is now:

$$k_{vsr} = \frac{nP_{s0}V_{sr0}^n A_s}{V_{sr}^{n+1}} \frac{dV_s}{dz}. \quad (8)$$

The functions $A_s(z)$ and $V_s(z)$ and their derivatives terms, dA_s/dz and dV_s/dz , will be determined experimentally as described in the following section.

At the other end of the spectrum, when the suspension dynamics is very fast, the pressure waves do not have time to reach the reservoir. Therefore, at high frequencies, the suspension behaves like a closed system formed by the air spring alone. The stiffness in this case is given by Eq. (2).

We modeled the stiffness for these two extreme scenarios: very slow dynamics (low-frequency range) in which case the stiffness is given by Eq. (7), and very fast dynamics (high-frequency range) in which case the stiffness is given by Eq. (2). In the following, we will describe a fluid dynamics model for the general case. The mass flow from the air spring to the reservoir can be expressed by the continuity equation:

$$\dot{m} = -\dot{\rho}_s V_s - \dot{V}_s \rho_s \quad (9)$$

the flow being positive when filling the bellows.

The suspension air temperature was monitored experimentally in working conditions by means of a thermocouple. The results supported the hypothesis of an isothermal transformation. With this hypothesis, the air spring density variation with respect to time can be defined as follows:

$$\dot{\rho}_s = \frac{\dot{P}_s}{RT}, \quad (10)$$

where the ideal gas equation, $P_s = \rho_s RT$, has been assumed. Combining Eqs. (9) and (10) yields

$$\dot{P}_s = -\dot{m} \frac{RT}{V_s} - \dot{V}_s \frac{P_s}{V_s}. \quad (11)$$

The same steps followed to obtain Eq. (11) are now used at the reservoir end in order to link the mass flow rate to the reservoir pressure (\dot{V}_r is equal to 0 because the walls of the reservoir are assumed rigid):

$$\dot{P}_r = \dot{m} \frac{RT}{V_r}, \tag{12}$$

where P_r is the auxiliary reservoir pressure. The rate of change of reservoir pressure connected to a pipe is the same rate one would have in a discharge process [12], and may be written as

$$\dot{P}_r = -\frac{\gamma C_r}{2V_r} (P_r^2 - P_s^2), \tag{13}$$

where γ is the specific heat ratio and C_r the restriction coefficient defined as [13]

$$C_r = \frac{\pi D_p^4}{128\mu l_p}, \tag{14}$$

where l_p is the pipe length, D_p is the pipe’s cross-section diameter, and μ the dynamic viscosity of air. Previous work on the type of flow (taking into account the size of the pipes and the amplitude and frequency of the experimental excitation signal) allow us to consider an incompressible-fully developed-laminar flow (Hagen-Poiseuille flow), in particular, Mach number $M < 0.3$ and Reynolds number $Re < 2300$. Eqs. (11) and (12) are combined to yield

$$\dot{P}_s = -\dot{P}_r \frac{V_r}{V_s} - \dot{V}_s \frac{P_s}{V_s}. \tag{15}$$

Two additional equations are now incorporated to complete the analytical model. One is the variation of the air spring force with respect to time, and can be obtained from the derivative of Eq. (1):

$$\dot{F} = \dot{P}_s A_s + P_s \dot{A}_s. \tag{16}$$

The other is Newton’s second law:

$$M\ddot{x} + Mg - F = 0 \tag{17}$$

with M being the sprung mass, x its dynamic response, and g the acceleration due to gravity. The variations of the air spring effective area and volume with respect to time (\dot{A}_s and \dot{V}_s) that appear in Eqs. (15) and (16) can be written as

$$\dot{A}_s = \frac{dA_s}{dz} \frac{dz}{dt} = A'_s(\dot{x} - \dot{y}), \tag{18}$$

$$\dot{V}_s = \frac{dV_s}{dz} \frac{dz}{dt} = V'_s(\dot{x} - \dot{y}). \tag{19}$$

Eq. (15) is combined with Eq. (19) to obtain the first equation in the system below. The second equation of this system is equal to Eq. (13). The third equation in the system is obtained combining the derivative with respect to time of Eq. (17) with Eqs. (16) and (18). With all these expressions put into order, one finally has the following system of differential equations:

$$\begin{cases} \dot{P}_s = -\dot{P}_r \frac{V_r}{V_s} - V'_s \frac{P_s}{V_s} (\dot{x} - \dot{y}), \\ \dot{P}_r = -\frac{\gamma C_r}{2V_r} (P_r^2 - P_s^2), \\ M\ddot{x} = \dot{P}_r A_s + P_s A'_s (\dot{x} - \dot{y}). \end{cases} \tag{20}$$

This system has only three unknown functions of time, P_s , P_r , and x . The other elements are known parameters (M , V_r , C_r , and y) or functions that have to be determined experimentally ($A_s(z)$ and $V_s(z)$).

2.1. Experimental characterization of the air spring

The previously presented model depends on two functions of height that need to be determined experimentally. These functions are the air spring effective area and the air spring volume. Two trials were performed in order to characterize the suspension. The setup included neither the tank nor the connecting pipe.

First, to determine the air spring effective area, the spring was locked at its upper end, and its lower end, fixed by the hydraulic gag, was subjected to the displacement excitations. The test input motion was a monotonic displacement in which the height z changes from 0.09 to 0.175 m. The air spring pressure was kept constant by means of a pressure control valve. This trial was performed for three constant pressures: 2, 3, and 4 bar. The effective area is the ratio between the exerted force as measured from the hydraulic actuator load cell, and the constant pressure at which the test was carried out.

Then, to determine the variation of the air spring volume with height, a pressure-controlled pump was used to fill the spring with water keeping the pressure constant. The height z was again varied as in the previous trial from 0.09 to 0.175 m. This means that the pressure-controlled pump had to fill or empty the spring, depending on that height, to maintain its pressure at a constant value. This procedure was carried out for several values of the air spring height. For each height, the water inside the air spring was retrieved and weighed to measure the volume at that particular height. The tests were performed for different pressures (the same as were used for the effective area case).

Fig. 1a shows the effective area versus height for the three pressures, and Fig. 1b volume versus height for the same three pressures. As can be seen both area and volume are almost independent of pressure, and, importantly, the two functions are fairly close to linear.

2.2. Numerical solution

The system of differential equations (20) were solved numerically by substituting the experimental characterization described in the previous section. The processing was done in the Matlab Simulink environment [14].

The principal block diagram for the model is shown in Fig. 2. The model input function is the excitation y and the output functions are the air spring and reservoir pressures (P_s and P_r) and the dynamic response (x). This main scheme is divided into three secondary blocks representing the three differential equations of system (20). These three secondary blocks yield the unknown functions x , P_s , and P_r , which are then re-introduced to their own and the other blocks in a process of iteration, as shown in Fig. 2. Besides these functions, the other experimentally obtained constants or functions of the height are substituted into each particular block.

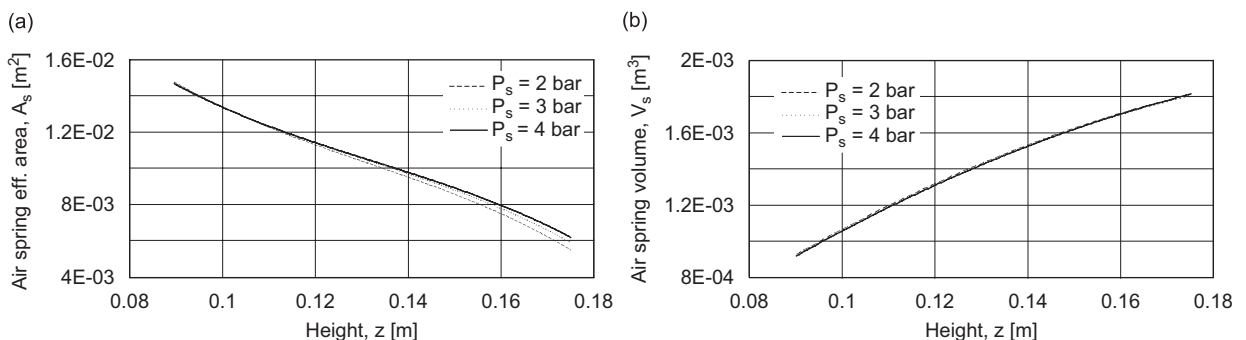


Fig. 1. Experimental characterization of (a) the air spring effective area and (b) the air spring volume.

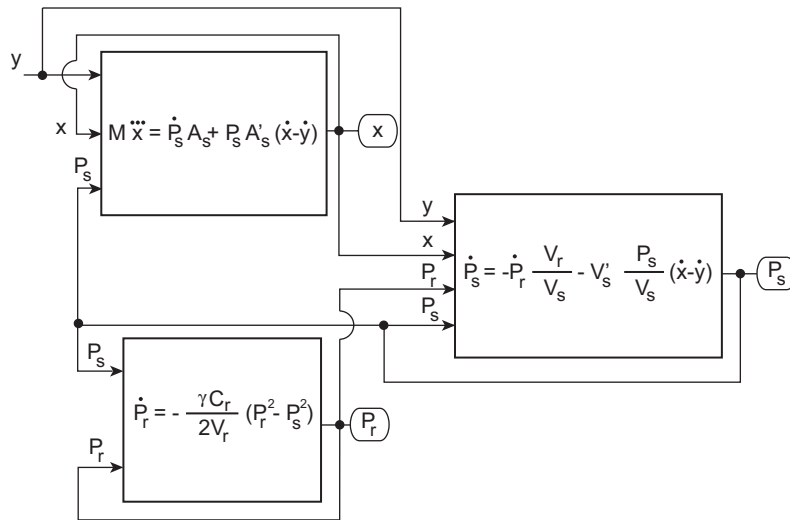


Fig. 2. General Simulink block diagram for the nonlinear model of the pneumatic suspension.

The pneumatic suspension’s stiffness is first simulated. Four different types of pipes represented by their C_r coefficients are used. A frequency range from 0.1 to 25 Hz was used in the analysis. The results of this simulation can be seen in Fig. 3. All curves show relatively constant stiffness zones at low and high frequencies and an intermediate transition zone connecting them. This stiffness behavior pattern is repeated for every C_r coefficient. Nevertheless, the transition frequencies grow with C_r . The suspension’s Carding diagram is plotted in Fig. 4 for every type of pipe. These diagrams are obtained by simulating using a stroke of ± 5 mm above and below the air spring initial height z_0 . Four different diagrams (for four different excitation frequencies) are presented for each C_r coefficient.

The Carding diagrams show the variation of stiffness (overall slope of the loop) and of damping (area inside the loop) with frequency. Damping grows with frequency up to a maximum value from which damping decreases as frequency grows. The corresponding transition frequency grows with C_r . The frequency range where damping grows can also be observed in the Bode plot phase diagrams of Fig. 3. One sees that, at low and high frequencies, the signals $F(s)$ and $Z(s)$ are in phase opposition. At intermediate frequencies, there is a time delay between $F(s)$ and $Z(s)$ for all the stiffness curves, with roughly the same phase curve shape being repeated at earlier or later frequencies depending on the value of C_r . The greater the C_r pipe coefficient, the higher the frequency needed to reach the high-frequency limit.

The suspension response to step displacement inputs is now analyzed for the two extreme C_r values. Two different step displacement sizes have been used: 10 and 2.5 mm. Results are shown in Fig. 5. It is easy to note that the suspension configuration for the lower C_r coefficient shows a higher stiffness, and therefore a higher natural frequency, than the system with higher C_r coefficient.

The pneumatic suspension’s transmissibility may finally be obtained. The results have been focused on the frequency range from 0.5 to 7 Hz. This simulation is shown in Fig. 6. The C_r influence on the suspension eigenfrequencies (already seen in Fig. 5) is again detected.

3. Linearized model

In this section, we will present a first-order Taylor series expansion of the nonlinear differential equations of Section 2. This Taylor series is obtained in the neighborhood of the static equilibrium point denoted by superscript st and defined by the following values:

$$\begin{aligned} \dot{m}^{\text{st}} &= 0, & A_s &= A_s^{\text{st}}, & z^{\text{st}} &= z_0, \\ P_s &= P_r = P_r^{\text{st}} = P_s^{\text{st}}, & \dot{P}_s^{\text{st}} &= 0, & \dot{P}_r^{\text{st}} &= 0, \end{aligned}$$

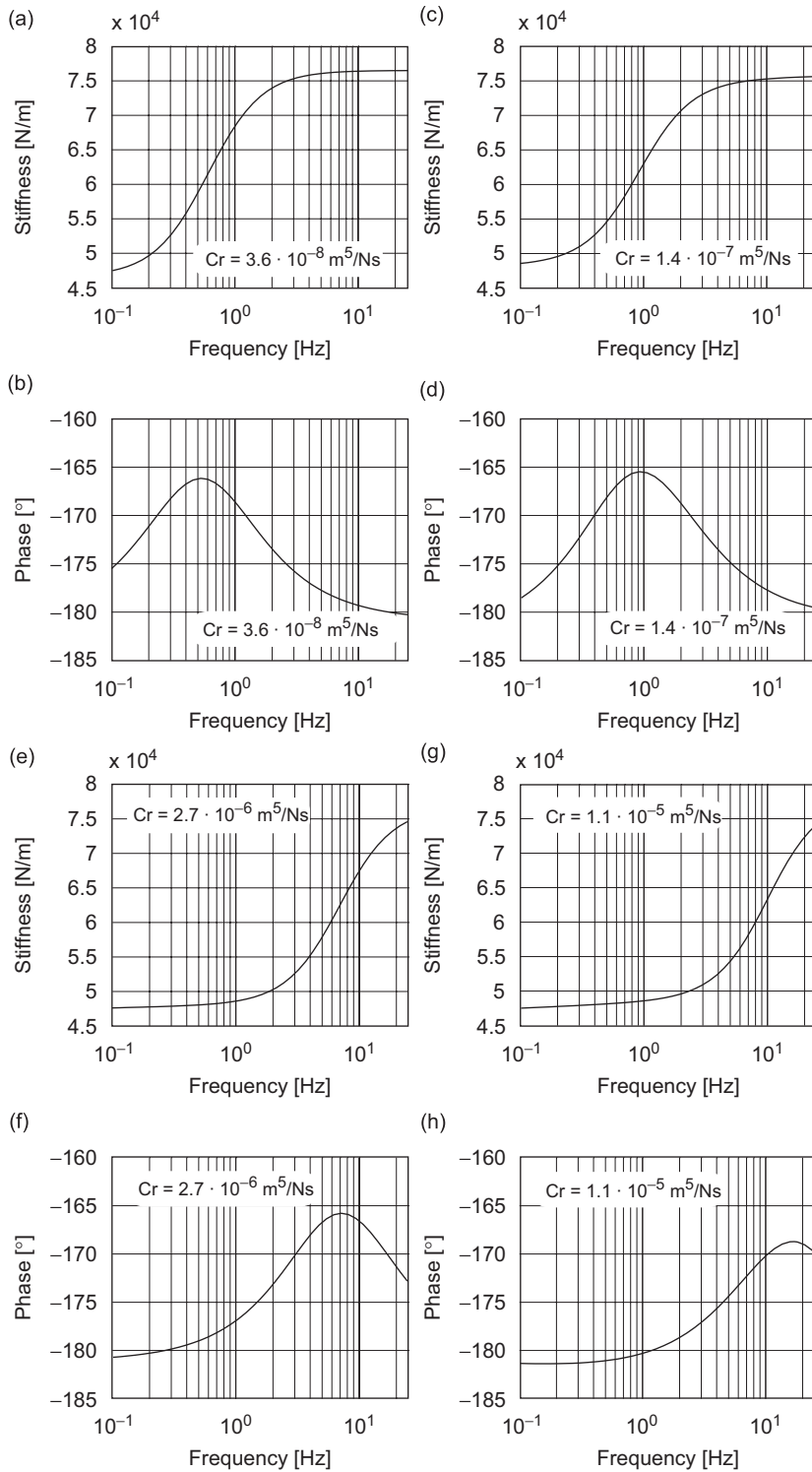


Fig. 3. Nonlinear simulation (stiffness modulus and phase diagrams) for the suspension frequency response: (a) and (b) for $C_r \approx 10^{-8}$; (c) and (d) for $C_r \approx 10^{-7}$; (e) and (f) for $C_r \approx 10^{-6}$; (g) and (h) for $C_r \approx 10^{-5}$.

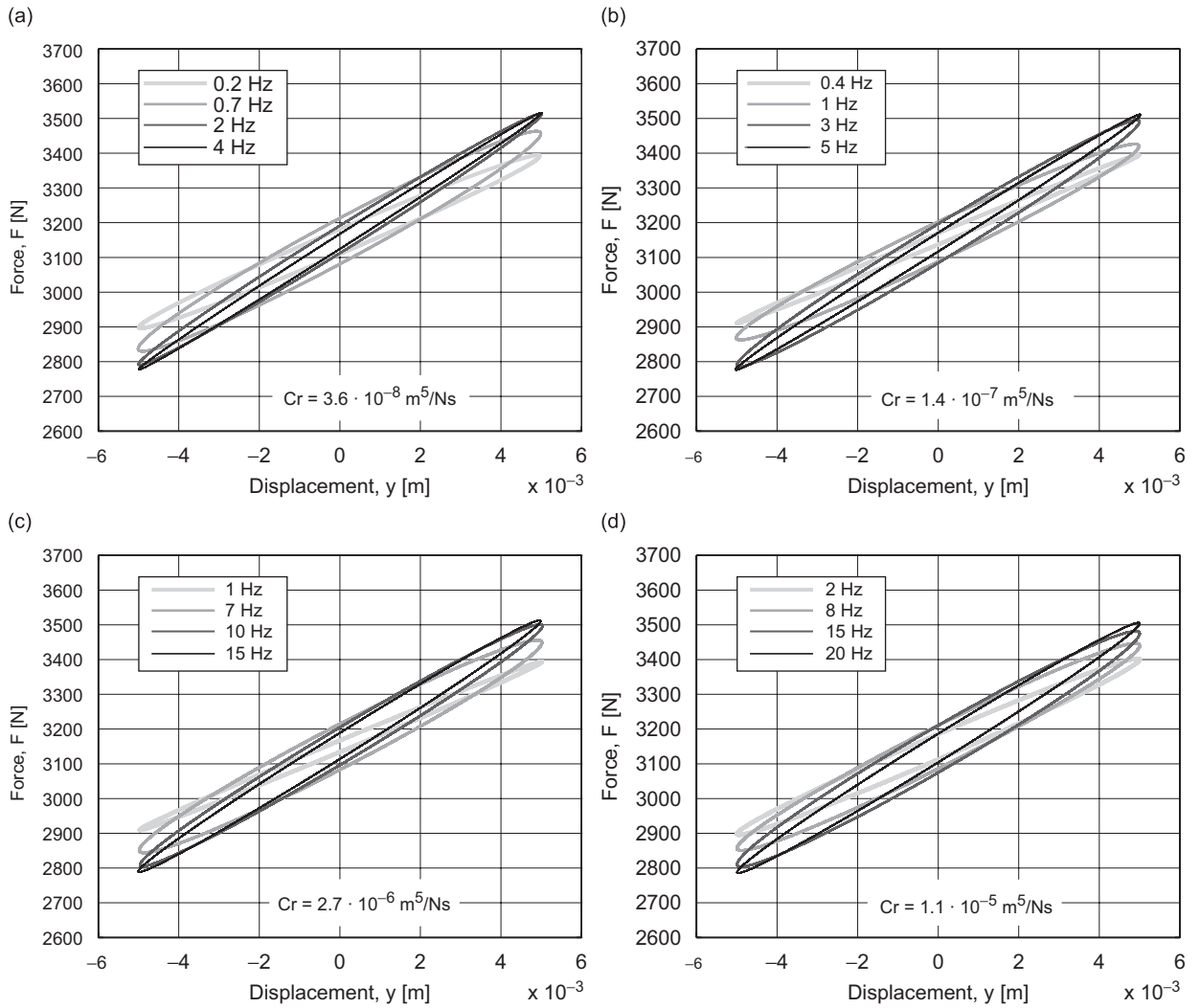


Fig. 4. Nonlinear simulation for the suspension Carding diagram: (a) for $C_r \approx 10^{-8}$; (b) for $C_r \approx 10^{-7}$; (c) for $C_r \approx 10^{-6}$; (d) for $C_r \approx 10^{-5}$.

$$A_s^{\text{st}} = \lambda, \quad V_s = V_s^{\text{st}}, \quad V_s^{\text{st}} = \kappa, \quad \dot{F}^{\text{st}} = 0, \quad \dot{z}^{\text{st}} = (\dot{x} - \dot{y})^{\text{st}} = 0.$$

The linearized version of the system of differential equations is the following:

$$\dot{P}_s = -\dot{P}_r \frac{V_r}{V_s^{\text{st}}} - \kappa \frac{P_s^{\text{st}}}{V_s^{\text{st}}} (\dot{x} - \dot{y}), \tag{21}$$

$$\dot{P}_r = -\frac{\gamma C_r P_s^{\text{st}}}{V_r} (P_r - P_s), \tag{22}$$

$$M\ddot{x} = A_s^{\text{st}} \dot{P}_s - \lambda P_s^{\text{st}} (\dot{x} - \dot{y}). \tag{23}$$

Applying Laplace's transform to Eqs. (21)–(23), one obtains the stiffness transfer function as follows:

$$\frac{F(s)}{Z(s)} = -\frac{s(K_{AS} + K_{VS}) + WK_{VS}(1 + K_{AS}/K_{VSR})}{s + W(K_{VS}/K_{VSR})}, \tag{24}$$

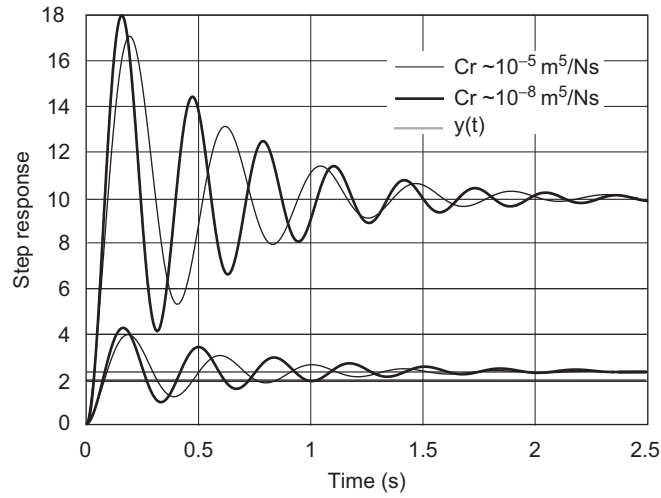


Fig. 5. Nonlinear simulation for the suspension step response.

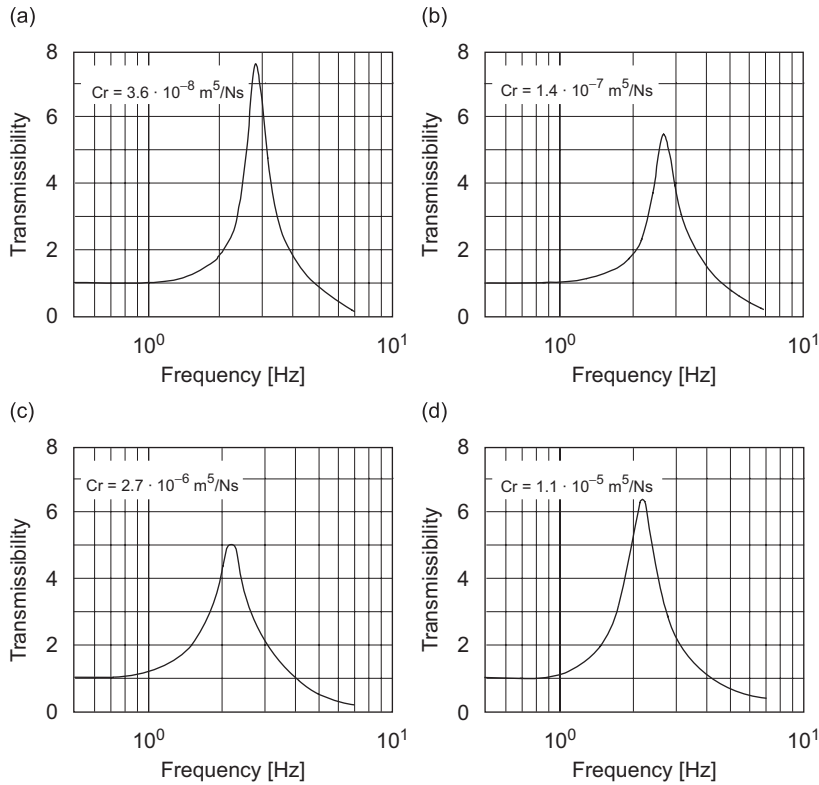


Fig. 6. Nonlinear simulation for the suspension transmissibility: (a) for $C_r \approx 10^{-8}$; (b) for $C_r \approx 10^{-7}$; (c) for $C_r \approx 10^{-6}$; (d) for $C_r \approx 10^{-5}$.

where $F(s)$ is the Laplace transform of $F(t)$, $Z(s)$ is the Laplace transform of $z(t) = x(t) - y(t) + z_0$, W is defined as $W = \gamma C_r P_s^{st} / V_r$, and the terms K_{AS} , K_{VS} , and K_{VSR} are defined as

$$K_{AS} = -P_s^{st} \lambda = k_{as}|^{st}, \tag{25}$$

$$K_{VS} = \frac{P_s^{st} A_s^{st}}{V_s^{st}} \kappa = k_{vs}|^{st}, \tag{26}$$

$$K_{VSR} = \frac{P_s^{st} A_s^{st}}{V_s^{st} + V_r} \kappa = k_{vsr}|^{st} \tag{27}$$

and therefore the spring stiffness and suspension stiffness defined in Eqs. (4) and (7) are now written as

$$K_S = k_s^{st} = K_{AS} + K_{VS}, \tag{28}$$

$$K = k^{st} = K_{AS} + K_{VSR}. \tag{29}$$

The linearized Eqs. (21)–(23) written in the Laplace domain are also used to obtain the transmissibility transfer function. This function is the ratio between the response $X(s)$ and the excitation $Y(s)$:

$$\frac{X(s)}{Y(s)} = \frac{s((K_{AS} + K_{VS})/M) + W \frac{K_{VS}}{M} (1 + K_{AS}/K_{VSR})}{s^3 + s^2(WK_{VS}/K_{VSR}) + s((K_{AS} + K_{VS})/M) + W \frac{K_{VS}}{M} (1 + K_{AS}/K_{VSR})}. \tag{30}$$

It is convenient to write this last equation in a dimensionless form. For this purpose, one defines the dimensionless parameters θ and ε :

$$\theta = \sqrt{\frac{K_{AS} + K_{VS}}{K_{AS} + K_{VSR}}}, \tag{31}$$

$$\varepsilon = \frac{W}{\omega_s \theta^2} \frac{K_{VS}}{K_{VSR}}, \tag{32}$$

where $\omega_s = \sqrt{K_S/M}$. These two parameters are inserted into Eq. (30) yielding the dimensionless transmissibility transfer function:

$$\frac{X(s)}{Y(s)} = \frac{s(1/\omega_s \varepsilon) + 1}{s^3(1/\omega_s^3 \varepsilon) + s^2(\theta^2/w_s^2) + s(1/\omega_s \varepsilon) + 1}. \tag{33}$$

These expressions will be used next to obtain some conclusions about the behavior of the pneumatic suspension. In Fig. 3 of the previous section, the suspension stiffness was simulated by the nonlinear model. It was observed that the stiffness may be divided into two zones corresponding to low and high frequencies. All the stiffness curves for the four different values of C_r rise from a lower limiting value at low frequencies to an upper limiting value at high frequencies. These two limiting values do not depend on C_r , and correspond to those obtained with the simplified models of Section 2. In particular, the low-frequency stiffness coincides with that of Eq. (7), and the high-frequency stiffness with that of Eq. (4). These limiting values of stiffness of those two equations can also be obtained from the linear model. At low frequencies, the Laplace transform of the stiffness tends to

$$\left. \frac{F(s)}{Z(s)} \right|_{s \rightarrow 0} = K_{AS} + K_{VSR} \tag{34}$$

which gives a value of stiffness equal to K . At high frequencies, the Laplace transform of the stiffness tends to

$$\left. \frac{F(s)}{Z(s)} \right|_{s \rightarrow \infty} = K_{AS} + K_{VS} \tag{35}$$

which gives a value of stiffness equal to K_S . The transitions between these two values take place at frequencies that depend on the coefficient C_r .

In Fig. 6, the eigenfrequency corresponding to the largest C_r value is close to the lowest achievable. Indeed, this eigenfrequency may be calculated approximately by assuming the pneumatic suspension stiffness in this situation to be the linear model stiffness at low frequencies, K . Similarly, the eigenfrequency corresponding to the smallest C_r coefficient is close to the highest achievable, and can be calculated approximately by assuming the stiffness in this situation to be K_S . Consider now the dimensionless parameter ε related to the pipe restriction coefficient that were defined above. The two limits as ε tends to zero and

to infinity yields

$$\left. \frac{X(s)}{Y(s)} \right|_{\varepsilon \rightarrow 0} = \frac{1}{s^2 1/\omega_s^2 + 1}, \quad (36)$$

$$\left. \frac{X(s)}{Y(s)} \right|_{\varepsilon \rightarrow \infty} = \frac{1}{s^2 \theta^2/\omega_s^2 + 1} = \frac{1}{s^2 1/\omega^2 + 1} \quad (37)$$

defining ω as $\sqrt{K/M}$. This limits make it possible to understand the meaning of the kind of pipe connection between the reservoir and the air spring. The limit as ε tends to zero corresponds to a small coefficient C_r , and Eq. (36) is that of a typical non-damped system with an equivalent stiffness K_S , and it can be seen that the system behaves as an air spring suspension with no contribution from the reservoir. The limit as ε tends to infinity, Eq. (37), means that, for large values of the coefficient C_r , the behavior is that of a non-damped system with an equivalent stiffness K , corresponding to the suspension working as the air spring with an increased volume coming from the reservoir.

4. Experimental results

The suspension stiffness, damping, and transmissibility are now measured with an experimental air spring suspension for comparison with our previous development of this system model. The pneumatic suspension we considered consists of three principal parts as it was said before. The first is the air spring itself (M/31062 of Norgren). This is a two-bellow air spring, with 90 mm total stroke, made of reinforced rubber (SBR), and functional from -40 to 70°C and up to 8 bar. The second component is a 21 capacity steel tank. And the third is a nylon pipe connecting the first two elements. The dimensions of this pipe were changed in several ways (according to the ones whose C_r coefficient was selected in the models) for their influence to be studied. Indeed, the sizes of the pipe, tank, and air spring were found to be the most important design parameters in determining the suspension's behavior.

Fig. 7 shows the experimental setup. Two types of trials were performed on a displacement controlled hydraulic actuator (MTS 810): the pneumatic suspension stiffness was measured with the setup shown in Fig. 7a, and the suspension damping and the sprung mass absolute response, i.e., the system's transmissibility, was measured with the setup shown in Fig. 7b. For the stiffness measurements, the top of the air spring is

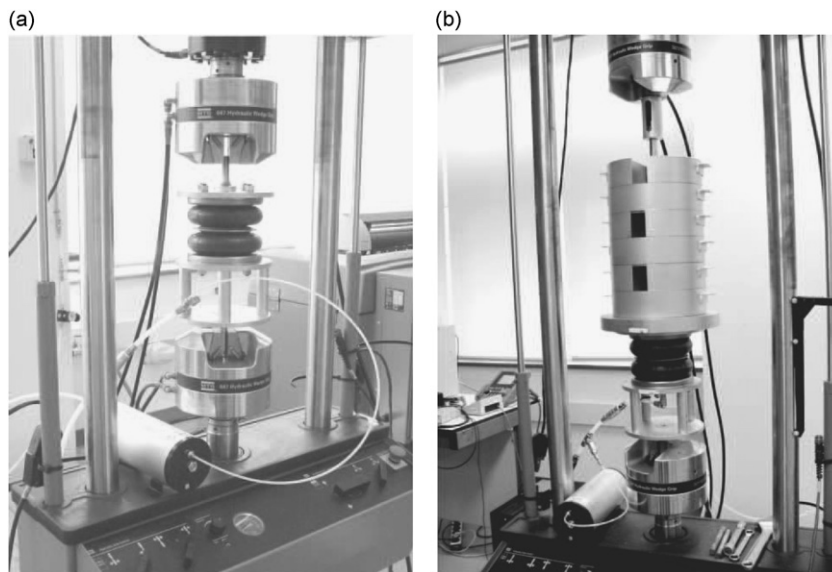


Fig. 7. Experimental setup: (a) stiffness measurements with no suspended mass; (b) damping and transmissibility measurements with suspended mass.

locked by the hydraulic actuator's upper gag, and the bottom gag exerts the excitation. For the transmissibility measurements, the upper gag holds a linear bearing that guides the sprung mass placed on top of the pneumatic suspension, and again the suspension excitation comes from the bottom gag.

The pipe sizes were selected with widths in the range 2.7–8 mm, and lengths of 0.5–2 m. The initial air spring height was set at 130 mm. The air spring initial internal pressure was 3 bar for the stiffness measurements, and 1 bar for the transmissibility measurements, the latter internal pressure chosen to equilibrate the sprung mass static load (120 kg). With a higher initial pressure, a larger mass must be mounted. The sprung mass in the present trials was chosen as a function of the work space allowed by the hydraulic unit. The total air mass (including bellows, pipe, and tank) was held constant.

The displacement input signal for the stiffness trials was a 5 mm amplitude sine wave applied by the hydraulic actuator. The frequency range tested was 0.1–25 Hz. The output signal was the force wave as measured by the hydraulic actuator load sensor. The results will be presented for four different pipes characterized by their corresponding restriction coefficient C_r (the same as that in the models). Fig. 8 shows the suspension stiffness obtained using the nonlinear model, the linear model, and the experimental results. The stiffness is shown both in magnitude (Figs. 8a, c, e, and g) and phase (Figs. 8b, d, f, and h) for four different values of C_r . As can be seen in the figure, the behavior of the suspension at the workbench has been well predicted both by the nonlinear and the linear models. The experimentally obtained Carding diagrams are shown in Fig. 9. The diagrams are well in agreement with those of Fig. 4.

The test setup shown in Fig. 7b was used to measure the suspension damping (by means of the step response test). The hydraulic actuator provides a square signal that can be used as a step input. The frequency of that square signal was chosen to be slow enough for the attenuated output signal (sprung mass displacement) to be acquired properly. As in the nonlinear model simulation, two-step displacement sizes have been used in the experimental case: 10 and 2.5 mm. The results of this test can be seen in Fig. 10.

Fig. 11 shows the experimental and the linear model normalized step responses of the suspension for the smallest and the largest values of C_r (Figs. 11a and b, respectively). Table 1 presents the values of the suspension damping factor and eigenfrequencies calculated with the linear model for these two C_r values, together with the experimental values. The experimental dimensionless damping factor ζ was estimated by means of the logarithmic decrement technique [15], giving values for these damping factors from 0.119 to 0.085, where the lower values corresponding to pipes with larger and smaller C_r coefficients. One observes that the linear model was able to predict the suspension behavior quite well with respect to its stiffness, and hence its eigenfrequencies. The damping factor prediction was less accurate, however, although it is commonly found to be difficult to construct a good model to predict the damping. Indeed, in many cases this damping factor is determined experimentally.

Finally, the same set of four pipes were used for the transmissibility test, but now with a 1.5 mm sine wave input signal and a frequency range from 0.5 to 7 Hz. The displacement output signal was captured by an LVDT (Schaevitz DC-EC 2000) with ± 50 mm measurement range and 0.01 mm resolution assembled onto the sprung mass. Fig. 12 shows the transmissibility using the nonlinear model, the linear model and the experimental tests. This figure confirms that both models are in good approximation to the measured data.

5. Operation strategy

The modeling and testing of a pneumatic suspension have been useful in attaining a better understanding of its behavior, including the prediction of its dynamic response. However, as was seen, this type of suspension has many modes of operation depending on the choice of elements. One therefore requires an operational strategy to ensure getting the optimal performance of a suspension. Some examples of such strategies are presented in Refs. [9,16]. The former suggests using the well-known sky-hook principle and changing the size of an orifice, used as the air flow restriction element, according to the sign of the difference between the air spring and volume pressures. The latter suggests using a switchable viscous damper in series with a relaxation spring. Neither suggestion is straightforward to apply in practice. Another idea for suspensions of this type was put forward in Ref. [17]. The aim was to achieve a suspension whose dynamic response, as reflected in its transmissibility curves, has a special characteristic. Specifically, they look for the transmissibility curve with the lowest maximum, i.e., the strategy is to look for the best attenuation of the excitation. The idea is only practical, however, over a narrow frequency range. A meaningful improvement suggests itself if one observes

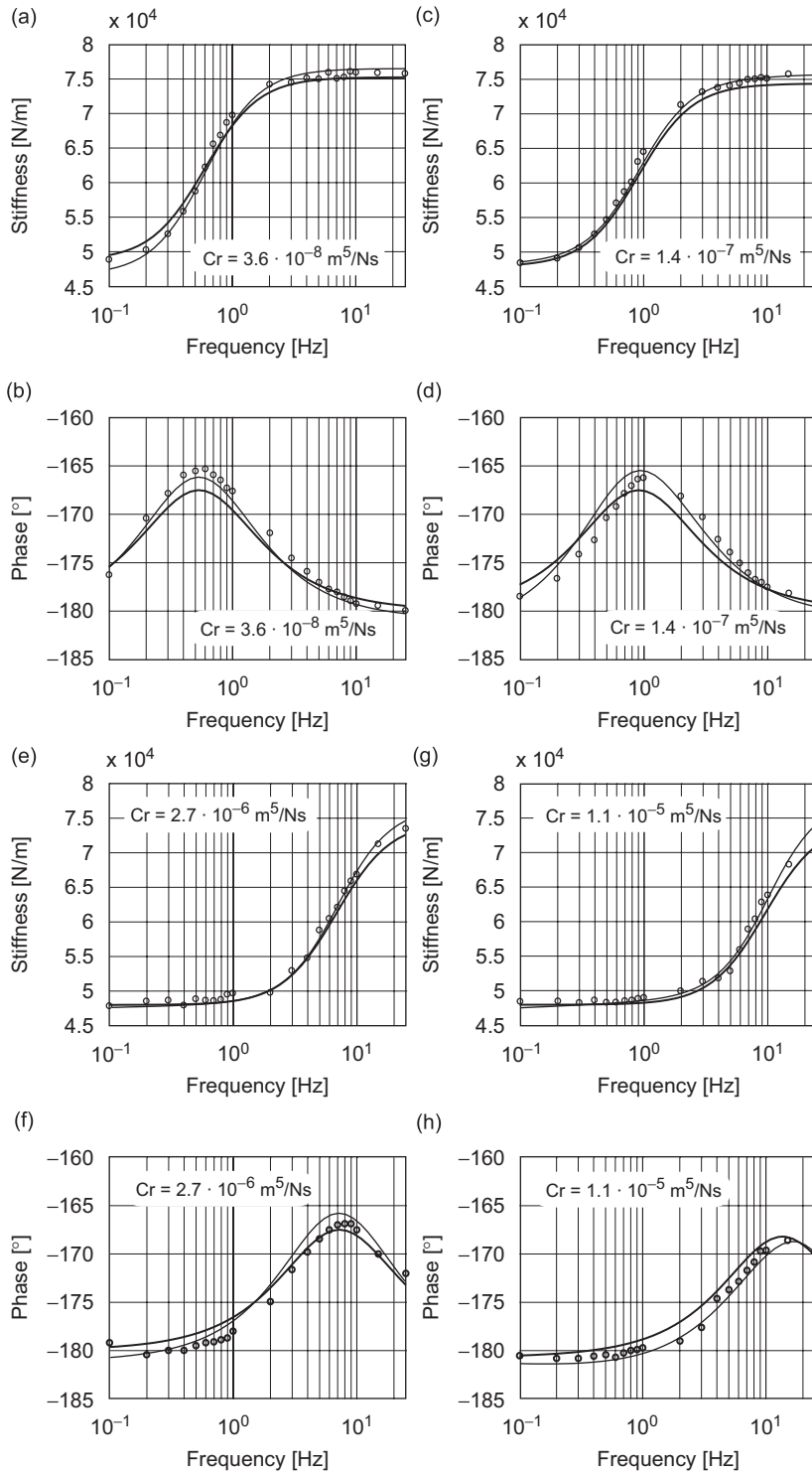


Fig. 8. Comparison of the nonlinear model (thin solid lines) and linear model (thick solid lines) with experiment for the stiffness (modulus and phase diagrams) of the pneumatic suspension: (a) and (b) for $C_r \approx 10^{-8}$; (c) and (d) for $C_r \approx 10^{-7}$; (e) and (f) for $C_r \approx 10^{-6}$; (g) and (h) for $C_r \approx 10^{-5}$.

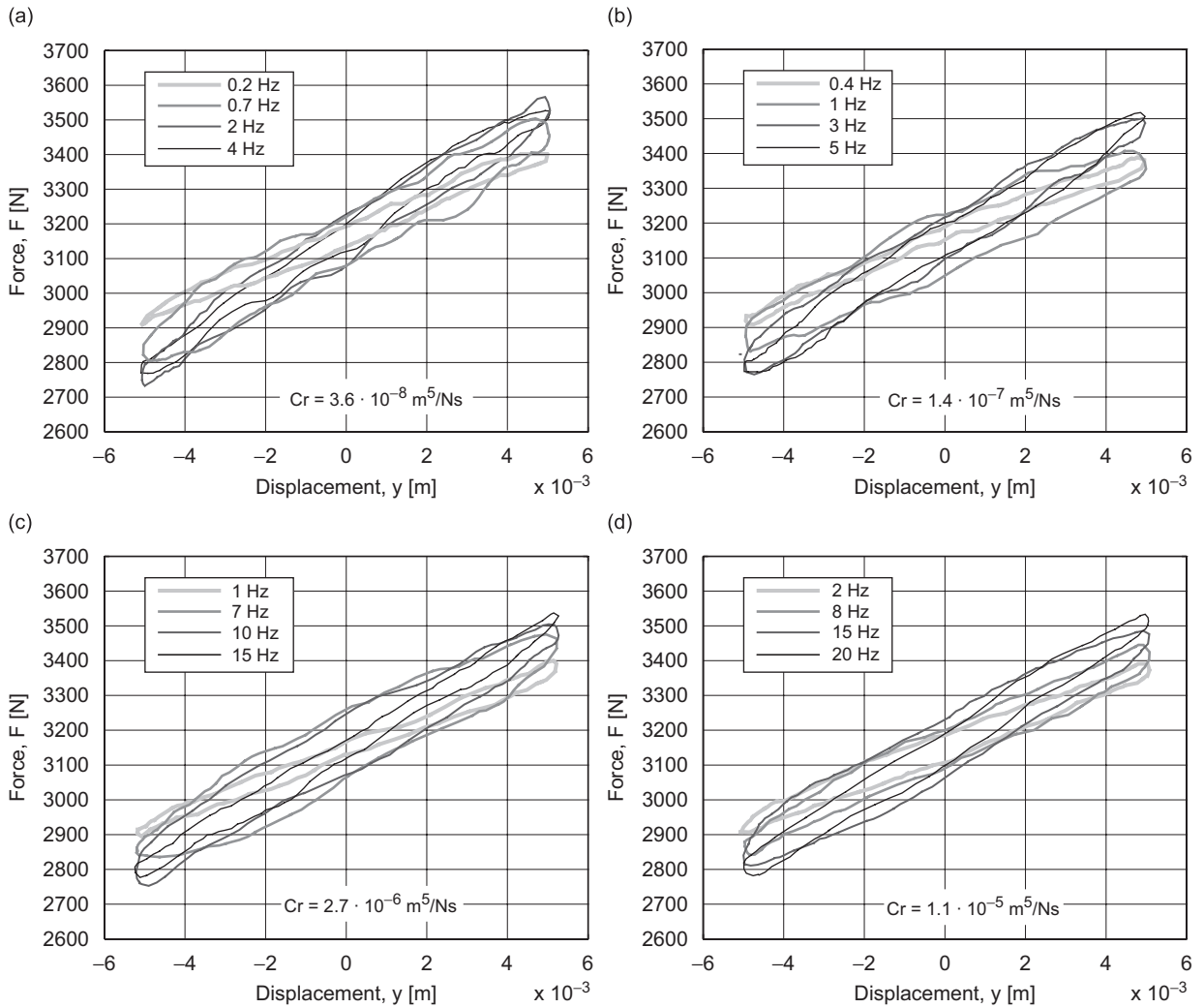


Fig. 9. Test results for the suspension Carding diagram: (a) for $C_r \approx 10^{-8}$; (b) for $C_r \approx 10^{-7}$; (c) for $C_r \approx 10^{-6}$; (d) for $C_r \approx 10^{-5}$.

the linear model transmissibility diagram (Fig. 13) in detail. In the magnitude diagram of that figure (Fig. 13a) one sees that there is a point through which all the curves pass. The difference between these curves, as was seen above, is related to the coefficient C_r , and therefore to the dimensionless parameter ε . The point can be calculated analytically in the model by assuming the following condition:

$$\frac{\partial |X/Y|}{\partial \varepsilon} = 0. \tag{38}$$

The frequency corresponding to that point is called the transition frequency (ω_{tr}), and is obtained as

$$\omega_{tr} = \omega_s \sqrt{\frac{2}{\theta^2 + 1}}, \tag{39}$$

while the value of the transmissibility modulus at this transition frequency is

$$\left| \frac{X}{Y} \right|_{tr} = \frac{\theta^2 + 1}{\theta^2 - 1}, \tag{40}$$

where θ is the dimensionless parameter defined in Eq. (31).

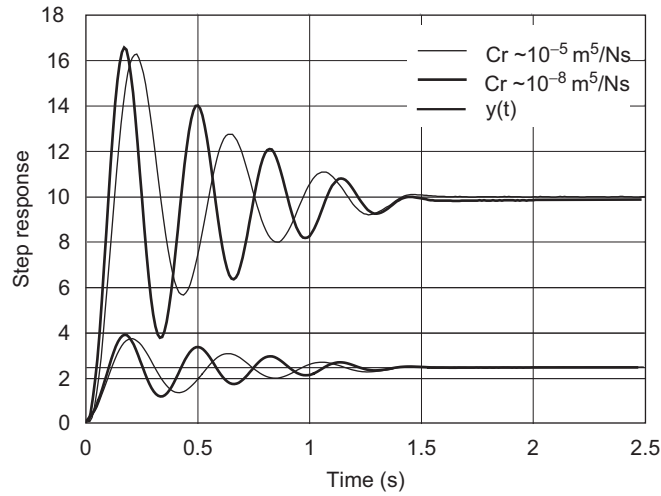


Fig. 10. Test results for the suspension step response.

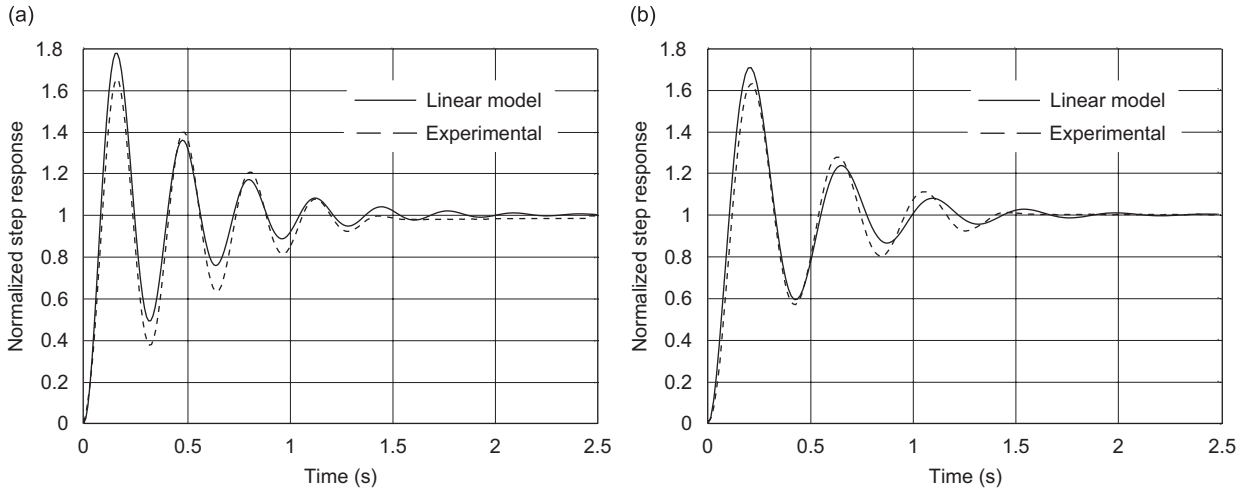


Fig. 11. Comparison of the linear model (solid lines) with experiment for the suspension step response of the pneumatic suspension: (a) for $C_r \approx 10^{-8}$; (b) for $C_r \approx 10^{-5}$.

Table 1

Comparison of the linear model and experimental results for the largest and the smallest values of the coefficient C_r studied

C_r	Method	f_n (Hz)	ξ	% Deviation f_n	% Deviation ξ
$\sim 10^{-5}$	Linear model	2.26	0.102	2.5	7.2
	Experimental	2.32	0.110		
$\sim 10^{-8}$	Linear model	3.054	0.075	1.0	11.7
	Experimental	3.088	0.085		

The identification of this transition point allows one to establish an operational strategy. On each side (left and right) of this point, there is a transmissibility curve whose amplification is the smallest least. These two curves do not, however, correspond to the same value of C_r . In other words, to get these results, one needs to use two different pipes. This may not be a problem if the transition point is used as a switching boundary.

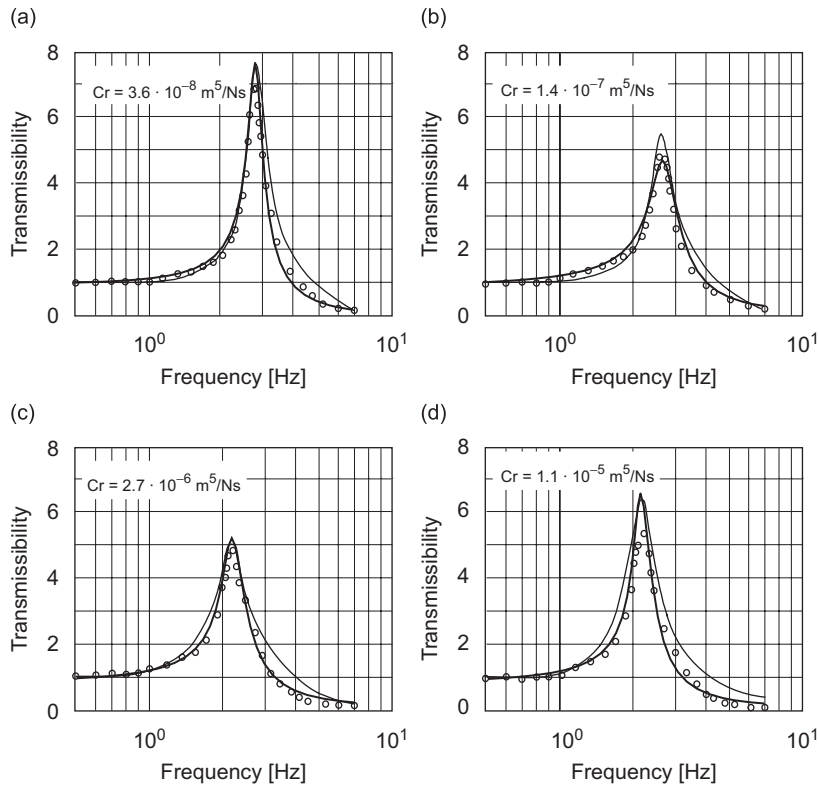


Fig. 12. Comparison of the nonlinear model (thin solid lines) and linear model (thick solid lines) with experiment for the transmissibility of the pneumatic suspension: (a) for $C_r \approx 10^{-8}$; (b) for $C_r \approx 10^{-7}$; (c) for $C_r \approx 10^{-6}$; (d) for $C_r \approx 10^{-5}$.

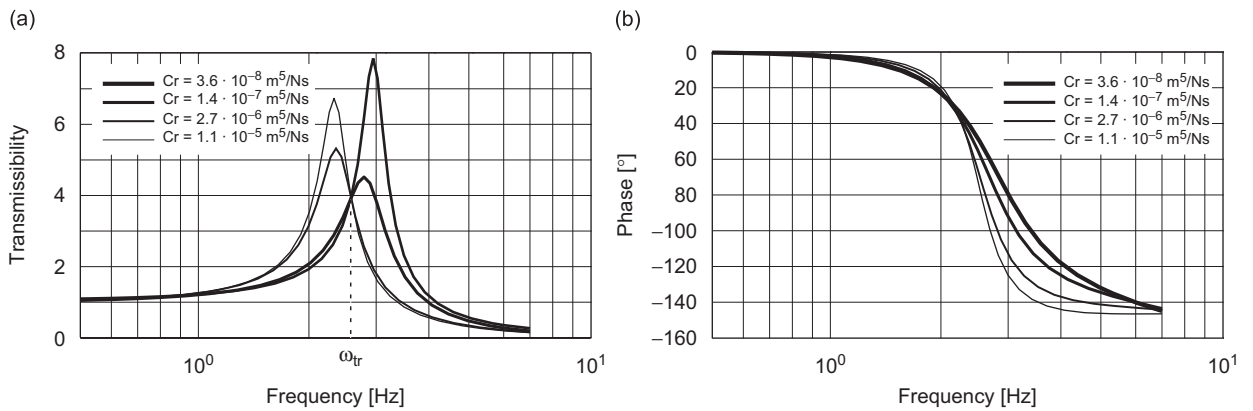


Fig. 13. Transition frequency in the transmissibility results (linear model).

One would then need two pipes for this strategy: one with the smallest and one with the largest value of the coefficient C_r . The transition point indicates where a change must be made from using one pipe to using the other. A switching valve would have to be used for this task, selecting the smaller C_r coefficient pipe if the excitation frequency was less than ω_{tr} , and the larger one otherwise.

Once the frequency ω_{tr} has been determined, the following task is to improve the features of the suspension, i.e., to achieve the smallest possible value of the transmissibility modulus (corresponding to that frequency ω_{tr}). The modulus, as Eq. (40) shows, is a function of the dimensionless parameter θ . Since the greater the value of this parameter, the smaller the modulus, the selection of the suspension elements must be aimed at

increasing the value of θ as much as possible. In other words, one must seek the greatest distance possible between the eigenfrequency values corresponding to the smallest and highest C_r coefficients in the transmissibility diagram by maximizing and minimizing the values of K_{VS} and K_{VSR} , respectively. This involves reducing the air spring volume V_s and increasing the reservoir volume V_r .

Reducing the air spring volume along with increasing the reservoir make it possible (as it has been argued above) to reduce the transmissibility modulus at transition frequency ω_{tr} . At the same time, this modulus reduction may improve the results of the control strategy when the aim is to filter single-frequency signals. The active control method just explained may also be useful when filtering vibrations caused by unbalanced rotating machines subjected to frequent start-stop cycles. Nevertheless, this active control strategy may be used as a basis in order to attenuate random vibrations. The details of the process are beyond the scope of this work, but it can be said that it will involve estimation of the excitation power spectral density (PSD), as well as criteria to switch between pipes of different sizes. To this end, real-time PSD estimation techniques (as proposed in Ref. [18]) will be needed.

6. Conclusions

We have presented an analytical model of the behavior of an air spring based on an experimental characterization. The solution of both the nonlinear model and its linearized version are well in agreement with our experimental measurements of the stiffness, damping factor, and transmissibility for a reasonable operation range of this suspension. It was shown that the dynamic behavior of the air suspension can be made more versatile by a convenient choice of the sizes of the its elements, in particular of the air spring and reservoir volumes. On the one hand, reducing the air spring volume increases the stiffness and hence also the highest eigenfrequency. And on the other hand, increasing the reservoir volume reduces the stiffness and hence also the lowest eigenfrequency.

Therefore, by implementing these changes in the elements of the suspension one can increase the difference between these two eigenfrequencies, i.e., one can increase the K_S/K ratio. The utility of this strategy would come into play if the air suspension were designed to work differently in two frequency regions. The working frequency range is naturally divided into two parts by a point at the “transition frequency” through which all the transmissibility curves pass. To achieve reasonable vibration attenuation, for low frequencies below this point one would choose the pipe with the smallest C_r coefficient, and for high frequencies above this point the pipe with the largest coefficient. This would require a control system capable of deciding and choosing the correct pipe to use according to the excitation frequency. If the suspension elements are not changed, the stiffness values K_{AS} , K_{VS} , and K_{VSR} are constant (if the initial working pressure is also constant). The value of the transition frequency, depends on the parameter θ which is a function of these three stiffness values. Furthermore, ω_{tr} depends on ω_s , i.e., on the sprung mass, so that varying this mass changes the value of ω_{tr} . Designing and implementing a control system that improves the suspension’s behavior according to the excitation frequency and the value of the initial sprung mass will be part of the authors’ ongoing work.

Acknowledgment

The authors are grateful for the support received from the Regional Project PBI05-020 entitled “Análisis y diseño de elementos neumáticos activos para el control de vibraciones” financed by the Consejería de Educación y Ciencia (Junta de Comunidades de Castilla-La Mancha).

References

- [1] E. Esmailzadeh, Optimization of pneumatic vibration isolation system for vehicle suspension, *Journal of Mechanical Design* 100 (1978) 500–506.
- [2] I. Hostens, H. Ramon, Descriptive analysis of combine cabin vibration and their effect on the human body, *Journal of Sound and Vibration* 266 (2003) 453–464.
- [3] I. Hostens, K. Deprez, H. Ramon, An improved design of air suspension for seats of mobile agricultural machines, *Journal of Sound and Vibration* 276 (2004) 141–156.

- [4] K. Deprez, D. Moshou, J. Anthonis, J. De Baerdemaeker, H. Ramon, Improvement of vibrational comfort on agricultural vehicles by passive and semi-active cabin suspensions, *Computers and Electronics in Agriculture* 49 (2005) 431–440.
- [5] R. Palej, S. Piotrowski, M. Stojek, Mechanical properties of an active pneumatic spring, *Journal of Sound and Vibration* 168 (2) (1993) 299–306.
- [6] G. Quaglia, M. Sorli, Experimental and theoretical analysis of an air spring with auxiliary reservoir, *Proceedings of the Sixth International Symposium on Fluid Control Measurement and Visualization*, Sherbrooke, Canada, 2000.
- [7] J.K. Baker, Vibration isolation, *Engineering Design Guides*, Vol. 13, Oxford University Press for the Design Council, 1975.
- [8] S. Koyanagi, The development of the air spring with variable nozzle, *Quarterly Report of Railway Technical Research Institute* 31 (3) (1990) 122–127.
- [9] R.J. Henderson, J.K. Raine, A two-degree-of-freedom ambulance stretcher suspension, *Proceeding Institution of Mechanical Engineers* 212 (Part D) (1998) 227–240.
- [10] C. Erin, B. Wilson, An improved model of a pneumatic vibration isolator: theory and experiment, *Journal of Sound and Vibration* 218 (1) (1998) 81–101.
- [11] B.I. Bachrach, Analysis of a damped pneumatic spring, *Journal of Sound and Vibration* 86 (2) (1983) 191–197.
- [12] E. Fermi, *Thermodynamics*, Dover Publications, New York, 1996.
- [13] I.H. Shames, *Mechanics of Fluids*, second ed., McGraw-Hill, New York, 1982.
- [14] MathWorks, Matlab 6.1.1., Copyright © by the MathWorks Inc., Natick, MA, 1999.
- [15] S.S. Rao, *Mechanical Vibrations*, third ed., Addison-Wesley, Reading, MA, 1995.
- [16] C.W. Stammers, The role of a relaxation damper in a semi-active suspension, in: *IMEchE Autotech 1993*, Birmingham, Paper C462/32/014, Mechanical Engineering Publications, London, 1993.
- [17] J.I. Soliman, D. Tajer-Ardabili, Self-damped pneumatic isolator for variable frequency excitation, *Journal of Mechanical Engineering* 8 (3) (1966) 284–293.
- [18] K. Kanazawa, K. Hirata, Parametric estimation of the cross-power spectral density, *Journal of Sound and Vibration* 282 (2005) 1–35.